SUPPORTING INFORMATION
"Measuring the size of biological nanostructures with Spatially Modulated Illumination Microscopy."

By Sonya Martin, Antonio Virgilio Failla, Udo Spöri, Christoph Cremer, Ana Pombo

In Part 1, we show a schematic of the SMI microscope set-up used (Fig. 4) and outline adjustments made to improve the laser-camera alignment and hence its sensitivity and detection. In Part 2, we describe the analytical size determination including the determination of site co-ordinates, the different methods used and the determination of the fit function that describes SMI-microscopy profiles. We also give details of a KDF Reader plug-in that allows SMI-microscopy image stacks to be opened using Image J software. In Part 3, we describe the sequential-subtraction methods used to determine sizes of structures by EM and SMI-microscopy, taking into account sectioning effects that can lead to underestimation of size. The first formulation presented (Fig. 5; previously published in Pombo *et al*., 1999) is used for lateral measurements on the EM, and the second (Fig. 6) is appropriate for measurements done axially on the SMI-microscope. Fig. 7 shows the results obtained for SMI-microscopy and EM measurements after correcting for sectioning effects (see also Fig. 3 in main text).

Part 1. SMI-microscope set-up

The SMI microscope set-up used has been described in detail in Albrecht *et al*., 2002. Here we show a simplified diagram of the set-up (Fig. 4A; adapted from Failla *et al*., 2002b) and a more detailed view of the area between the two objectives (Fig. 4Bi). Fig. 4Bii shows an example of how an image stack (160images) is obtained. The specimen is placed between a conventional microscope slide and coverslip. The slide is held between the two objectives on a piezoelectric stage. Immersion oil is applied to both the back face of the slide and the coverslip and an area of interest searched for and focused. The specimen is moved in the z direction 80 steps x 20 nm beyond the focal point and 160 images are collected in 20 nm steps as the specimen is moved back through the focal point to 80 x 20 nm beyond it in the other direction.

Improvements to microscope alignment and detection light path

In order to avoid ghost images and other stray light the detection light path was altered between the tube lens and the CCD chip. The microscope tube was widened to about 40 mm diameter, and covered on the inside with black velvet. Additionally, two iris diaphragms were inserted in order to block emitted light that does not fall on the CCD chip (Fig. 4A).

Part 2. Computer algorithms for analytical size evaluation of emission profiles obtained with SMI-microscopy

Methods

The sizes of pol II_O sites were determined from SMI-microscopy stacks of images using eight methods, differing in: (1) the determination of site co-ordinates and profiles, (2) removal of uninformative images at the two extremes of z-stacks, and (3) background subtraction (for summary see Table 1).

1. Determination of site co-ordinates and profiles

The co-ordinates of sites were selected visually at the centre of intensity (little variability between analysts is observed in the chosen centre of mass; from 23 sites, the centres of mass of 17 sites were recorded by three observers within 1 pixel, 3 were only recorded by two observers and 3 only seen by one observer; see also Pombo *et al*. (1999). For each site a stack of images, with dimensions 9x9x(160-180) centred on the co-ordinate, were extracted from the original KDF files using a Khoros Cantata workspace.

Methods 1-4

To compensate for noise and a possible drift of the sites' centre of intensity, a 3x3 mask is centred on the site co-ordinate in the focal plane (determined visually) and the emission profile is obtained from the average intensity of this mask at each image in the stack.

Methods 5-8

A 5x5 mask is centred on the site co-ordinate (determined visually) and used to extract a stack of images, with dimensions 5x5x(160-180) from the 9x9x(160-180) stack. The centre of intensity of the site is then defined as the position of maximum intensity within this 5x5 file for each image in the stack. This new intensity position is then used to produce the emission profile. [Note that this method will misbehave if an additional site lies within 300 nm of the central one (*i.e.* within 3 pixels), which is common with pol II_O sites.]

2. Removal of uninformative images at the two extremes of the z-stacks

An informative profile can usually be obtained from the 100 axial planes centred at the maximum intensity image at the focal plane. We tested whether removal of uninformative, noisy axial planes at the extremes of the profile improved the fit function.

Methods 1, 3, 5 and 7

No axial planes are removed *i.e*. the complete profile is used.

Methods 2, 4, 6 and 8

Axial planes from 50 images on either side of the image corresponding to the profile maximum were used. Images were removed from the stacks using Khoros Cantata.

3. Background subtraction

Methods 1, 2, 5 and 6

No background subtraction.

Methods 3, 4, 7 and 8

Background intensity was subtracted from the emission intensity values before determination of the fit function. The background subtraction routine assumes that the signal-to-noise ratio is equal to 80%; intensity values are measured at positions outside of the sections, the lowest 20% are averaged and this value is used as the background value. In this case, parameter L (mean background value) is deleted from the fit function that describes SMI-microscopy profiles (see below).

Table 1. Summary of the eight methods used to determine the size of pol II_O sites from SMI-microscopy image stacks

Method 3 (shaded) was chosen as the most suitable (see text for details).

	Method	1	2	3	4	5	6	7	8
Determination of site co-ordinates	3x3 mask	+	+	+	+				
	5x5 mask					+	+	+	+
Axial images used	All images	+		+		+		+	
	50 either side of the maximum		+		+		+		+
Background subtraction	No	+	+			+	+		
	Yes			+	+			+	+

Determination of fit functions that describe experimental SMI-microscopy

Each emission profile was analysed using Khoros Cantata to obtain a fit function and extract size and excitation wavelength parameters. The fit function describing the axial intensity distribution (AID) depends on a number of parameters of which A, D and F are dependent on the object size and C is proportional to the excitation wavelength (Failla *et al.*, 2002a).

$$AID = A \cdot \left(\frac{\sin\left(\frac{x - x_3}{B} \right)}{\frac{x - x_3}{B}} \right)^2 \cdot \left(\cos\left(\frac{x - x_2}{C} \right)^2 \right) + D \cdot \left(\frac{\sin\left(\frac{x - x_4}{E} \right)}{\frac{x - x_4}{E}} \right)^2 + F \cdot \cos\left(\frac{x - x_2}{C} \right)^2 + L$$

where: L is a mean background value calculated from the average background intensity; A, D and F are positive parameters that represent the amplitude of the fringe oscillation, the non-oscillating intensity of the inner portion of the profile and the background oscillation respectively; B, C and E are positive parameters proportional to the full width at half maximum (FWHM) of the modulating intensity distribution, the FWHM of the oscillating fringes and the FWHM of the inner non-oscillating part of the profile, respectively; and x_2, x_3, and x_4 are the positions of the maximum of the oscillating fringes (this maximum is arbitrary), the oscillating intensity distribution and the non-oscillating intensity, respectively.
The excitation wavelength can vary locally for individual sites, this is accounted for by parameter C, where $C = (2\pi N\Delta X)/\lambda$ [n is the index of refraction (1.54), and Δx is the distance between consecutive z-planes (20 nm)]. The size parameters are selected by the user (after examination of the profile; this choice is led by experience) to be used as starting parameters from which Khoros Cantata iteratively generates a fit function that best fits the experimental profile.
The fit function can fail to fit depending on the starting parameters inserted or on the user ability to adjust the parameters in an order of magnitude of 5% (our unpublished results). An appropriate fit function is chosen visually as one that is in reasonable agreement with the profile. Parameters A, D and F were extracted from the chosen fit functions and the modulation contrast [R=D/(A+D+F)] was calculated.

Size evaluations from the fit function
Calibration curves have been set up for different excitation wavelengths using virtual microscopy (Failla *et al.*, 2002a). The diameter of sites is extrapolated for values of R using the appropriate calibration curve (depending on λ).

Results; choosing the appropriate algorithm
Firstly, we found that using the maximum intensity in a 5x5 pixel mask as the co-ordinate of sites was inappropriate when more than one site lay within 5 pixels. Occasionally, especially with smaller/dimmer sites, peaks occurring at the edges of the profile are brighter than the site being measured and therefore distort the final profile. Secondly, removing uninformative planes at the profile edges did not facilitate the determination of the fit function and it added more computational time. Thirdly, we found background subtraction to be useful as it simplifies the analytical fit function. We therefore found method 3 (Table 1) to be the most appropriate for analytical size measurements from biological samples.

KDF Reader plug-in for Image J

The KDF reader allows SMI-microscopy image stacks to be visualised using the freely available Image J program. It is written in JAVA and its source code is based on the C++ routine used to save the image stack in the SMI Project (obtainable by contacting the authors). The data format written by the SMI Project differs slightly from the KDF specifications by Khoral Inc., because additional information on the

colour channels is stored with the image data. The 3D multicolour image stacks acquired by the SMI microscope occupy up to 700MB RAM, the KDF reader allows only part of the image to be opened *e.g.* single colour or specific 3D region of interest.

Part 3. Sequential-subtraction method to determine sizes of structures from sectioned samples.

The sequential-subtraction method of Weibel (1979) allows the radius of spheres contained in 3D specimens to be deduced from circular profiles in 2D images from 3D sections. During sectioning some spheres will be cut non-equatorially giving rise to polar caps whose radii will be smaller than the actual radii of the sphere. In a sample containing spheres of varying sizes (such as pol II_O sites), the proportion of polar caps that will appear from each size of object can be calculated (as in Figs. 5 and 6). Object sizes are separated into size categories and the proportion of polar caps is sequentially subtracted from each category, starting with the largest sized object.

Sequential-subtraction method to determine sizes from lateral measurements

This method has previously been adapted for lateral measurements of sites (*i.e.* measurements parallel to the plane of sectioning) contained in cryosections [transparent media, as gold probes access and are visualized throughout the thickness of sections;(Pombo *et al.*, 1999)], but here we present a graphical explanation (Fig. 5). In this example we show a sphere of radius (R) 20 nm in a section of thickness (T) 100 nm (Fig. 5A). R has been subdivided into 4 categories in intervals of 5 nm (ΔR). The red bar indicates that sites in this region will be measured with their true radii of 20 nm. Sites in the areas indicated by pink and fawn bars will be measured as <20 nm. Fig. 5B shows this graphically, for sites of 20 nm radius. In a 100 nm thick section, 90% will be measured as 15-20 nm, 6% as 10-15 nm, 3% as 5-10 nm and 1% as 0-5 nm. The frequency (f) of spheres in each size category depends on section thickness (T), the true radius of the spheres (R) and the size of the categories chosen to subdivide R (ΔR), and can be deduced using the equations in Fig. 5C. In a sample containing a mixture of sizes, the sequential-subtraction method is used; the contribution of caps is calculated for the largest size observed (which must represent a true R) and subtracted from the lower size classes. The process is then iterated for the next largest size to the smallest. In this way, a composite of profiles is derived, the histogram of true diameters is obtained and the weighted average diameter can be determined.

Sequential-subtraction method to determine sizes from axial measurements

The sequential-subtraction method was adapted for axially measured sites with SMI-microscopy (*i.e.* sizes measured perpendicular to the plane of sectioning; Fig. 6). In this example, we show a sphere of diameter (D) 40 nm in a section of thickness (T) 100 nm (Fig. 6A). D has been subdivided into 4 categories in intervals of 10 nm (ΔD). As with Fig. 5A, the red bar indicates that sites will be measured with their true diameter of 40 nm. Sites in the areas indicated by pink and fawn bars will be measured as <40 nm. Fig. 6B shows this graphically, for sites of 40 nm diameter in a 100 nm thick section; 65% will be measured as 30-40 nm and 12% as 20-30 nm, 10-20 nm and 0-10 nm. The frequency of sizes in each size category (f) depends on section thickness (T), on the true diameter of the spheres (D) and on the size of the categories chosen to subdivide D (ΔD) and can be deduced using the equations in Fig. 6C. Again, starting with the largest size category (which must represent a true diameter D), the contribution of incomplete sites arising from sectioning sites with

this diameter is determined and subtracted from the smaller categories. The process is then iterated as before.
After correcting the SMI-microscopy data for the contribution of incomplete sites, the frequency of sites smaller than 50 nm showed negative values (Fig. 7A and B, shaded bars), implying that SMI-microscopy was not sensitive enough to detect these small, incomplete sites. With EM, correction for the contribution of caps does not produce negative values (Fig. 7C), suggesting that all sites are detected.

References

Failla, A.V., Cavallo, A., and Cremer, C. (2002a). Subwavelength size determination by spatially modulated illumination virtual microscopy. Appl. Opt. *41*, 6651-6659.
Failla, A.V., Spöri, U., Albrecht, B., Kroll, A., and Cremer, C. (2002b). Nanosizing of fluorescent objects by spatially modulated illumination microscopy. Appl. Opt. *41*, 7275-7283.
Pombo, A., Hollinshead, M., and Cook, P.R. (1999). Bridging the resolution gap: Imaging the same transcription factories in cryosections by light and electron microscopy. J. Histochem. Cytochem. *47*, 471-480.
Weibel, E.R. (1979). Stereological methods: practical methods for biological morphometry. Academic Press: London, Vol. 1, pp.162-203.

Figure Legends

Figure 4. Schematic of SMI-microscope set-up and how image stacks are produced
A. The excitation laser is split and focused through two opposing objective lenses. The specimen is placed between the two objectives and is moved with nanometre precision using a piezoelectric control. Two iris diaphragms are used to block emitted light that does not fall on the CCD chip.
B. (i) The laser/objective configuration leads to production of a standing wave field between the two objectives. **(ii)** In order to produce an image stack, the specimen is moved away from the focal plane at position *b* to position *a*, and images are then collected at 20 nm intervals as the specimen is moved along the z direction from position *a*, through the focal point at position *b* to position *c*.

Figure 5. Sequential-subtraction method for sites measured laterally (EM)
When a 3D specimen containing spherical objects is sectioned it will give rise to incomplete spheres, which must be taken into account when determining the sizes of the objects. On the EM, sizes are measured laterally (*i.e*. in parallel to the plane of sectioning). This figure describes an adaptation of the sequential-subtraction method of Weibel (1979) for laterally measured sites [as described in Pombo *et al*., 1999].
A. Illustration of how an object of 20 nm radius (R) will be sectioned. Unless these objects are completely within the section or are cut equatorially they will be measured as smaller than their true radius and therefore will constitute polar caps.
B. Histogram of the frequencies of sizes produced by 20 nm radius objects in a section of 100 nm thickness.
C. Equations derived to calculate the frequencies of true sizes and polar caps.

Figure 6. Sequential-subtraction method for sites measured axially (SMI-microscopy)
The functions needed to calculate the contribution of incomplete sites for sites measured axially to the plane of sectioning with SMI-microscopy were derived in this example for a section thickness (T) of 100 nm and an object diameter (D) of 40 nm.
A. Illustration of how an object of 40 nm diameter (D) will be sectioned; only sites wholly contained in the section will be measured as their true diameter, and the others will inevitably lead to an underestimation of size.
B. Histogram of the frequencies of sizes produced by a 40 nm diameter object in a section of 100 nm thickness.
C. Equations derived to calculate the frequencies of true sizes and incomplete sites.

Figure 7. Size distribution of pol II_O sites obtained by SMI-microscopy and EM
A,B. The diameters of pol II_O sites were measured by SMI-microscopy in cryosections (~140 nm thick) labelled with a 2 layer protocol as for Fig. 2A-C (A) or with a 3-layer protocol using H5, rabbit anti-Ig Abs and Alexa Fluor 488 (B). Sizes were grouped into 10 nm ranges and frequencies expressed as a percentage of the total. Using the sequential-subtraction method for axial measurements (see Fig. 4) the contribution of incomplete sites arising from sectioning effects was evaluated for each size range. Solid bars show corrected size frequencies (weighted average diameter 81 and 89 nm for A and B, respectively; n=148 and 338), open bars show the proportion of incomplete sites that were detected and the shaded bars show undetected incomplete sites. The appearance of negative values after correction for incomplete

sites implies that SMI-microscopy is not detecting (or appropriately measuring) smaller sites.

C. Diameters of 105 clusters of gold particles marking pol II_O were measured in cryosections (~140 nm) labelled as in Fig. 2D. Sizes were grouped into 10 nm ranges and frequencies expressed as a percentage of the total. The contribution of caps was calculated using the sequential-subtraction method for lateral measurements (Fig. 6; open bars) and subtracted to give corrected frequencies (solid bars). Clusters had an average (weighted) diameter of 45 nm after correction for caps.

Note: The proportion of incomplete sites with SMI-microscopy is greater than that of caps with EM due to the effects of measuring axially and laterally. With axial measurements all sites that are not wholly contained within the section will constitute incomplete sites. However, for lateral measurements only sites that are more than halfway out of the section will constitute polar caps.

Martin S., Figure S4

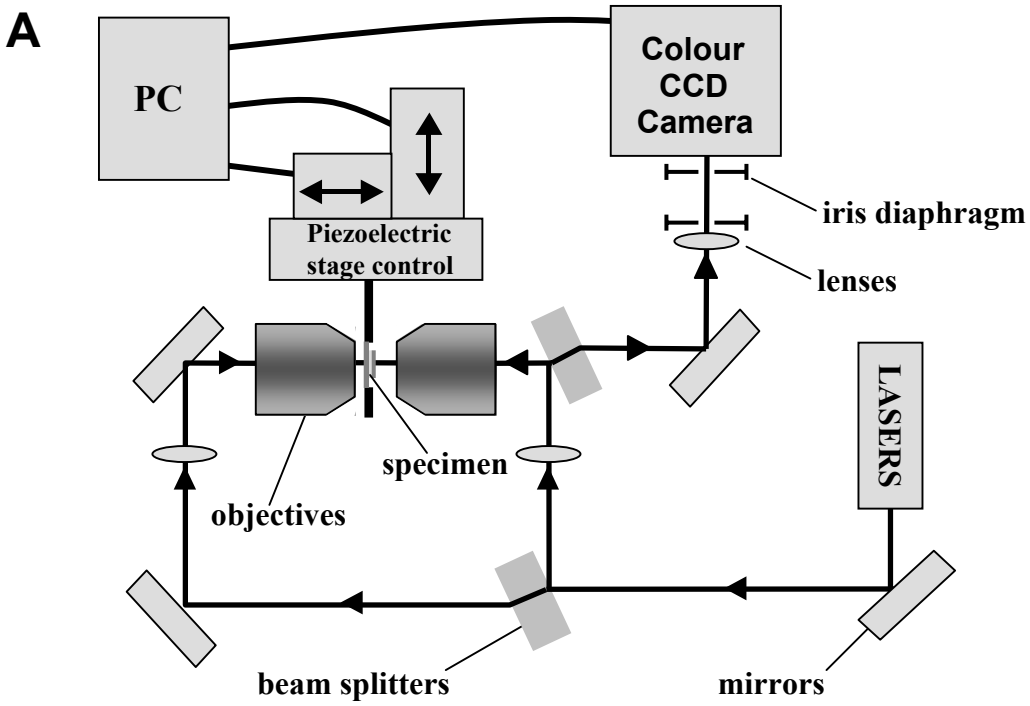

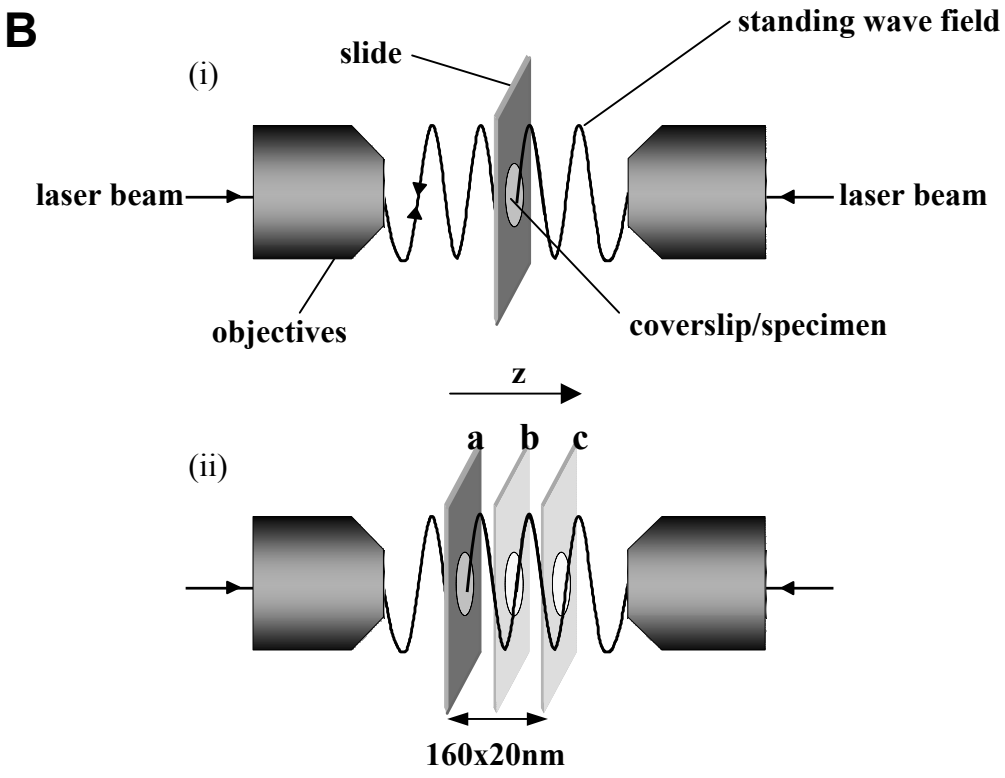

Martin S., Figure S5

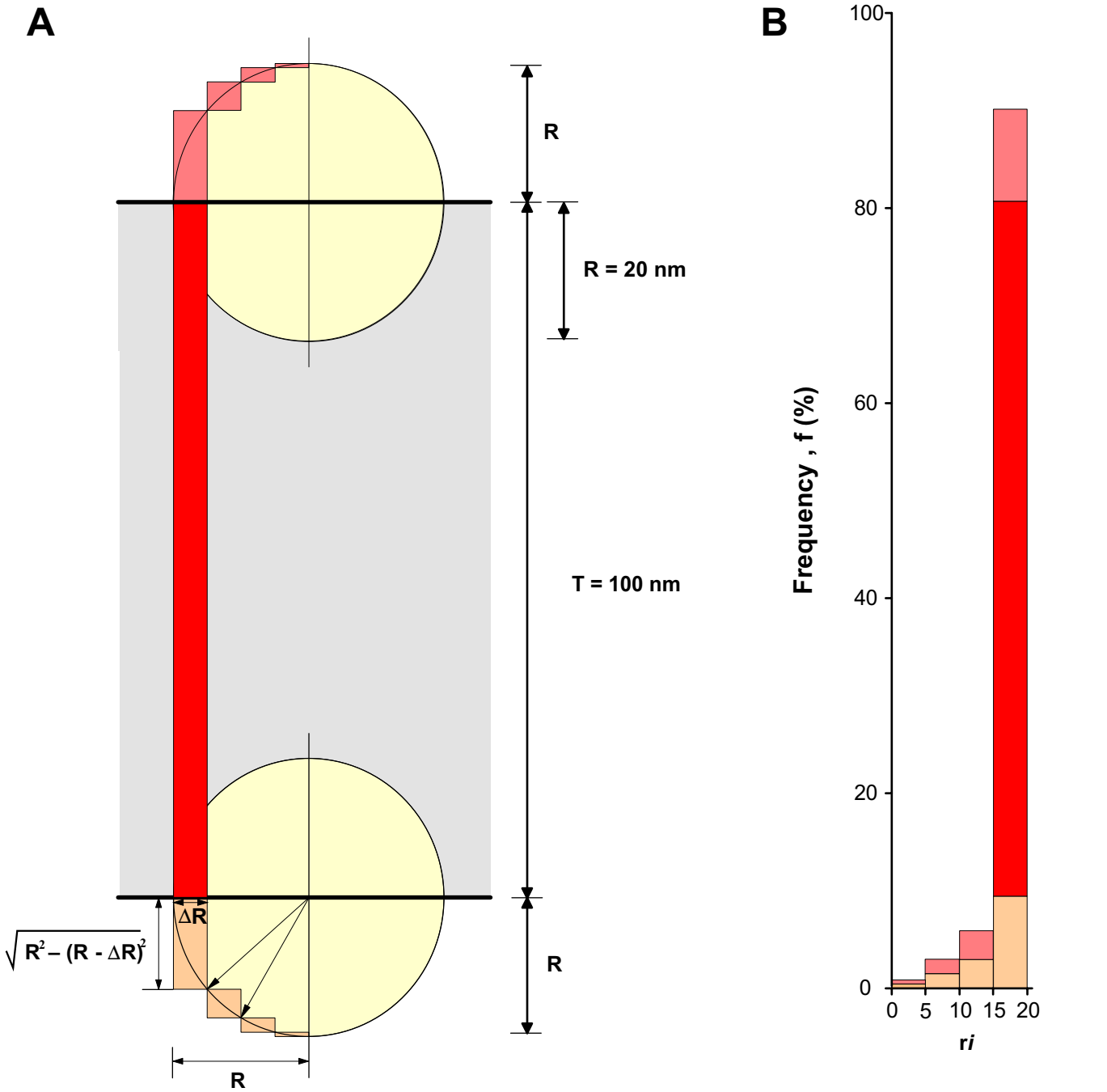

C

f = frequency
R = radius of object
T = thickness of section
r_i = size category
ΔR = class size

$r_i = R - i\Delta R$ where $\left(i = 1 \ldots \frac{R}{\Delta R}\right)$

for $R - \Delta R < r_i \leqslant R$

$$f(r_i) = \frac{2\sqrt{R^2 - (r_i - \Delta R)^2} + T}{T + 2R}$$

for $r_i \leqslant R - \Delta R$

$$f(r_i) = \frac{2\left(\sqrt{R^2 - (r_i - \Delta R)^2} - \sqrt{R^2 - r_i^2}\right)}{T + 2R}$$

Martin S., Figure S6

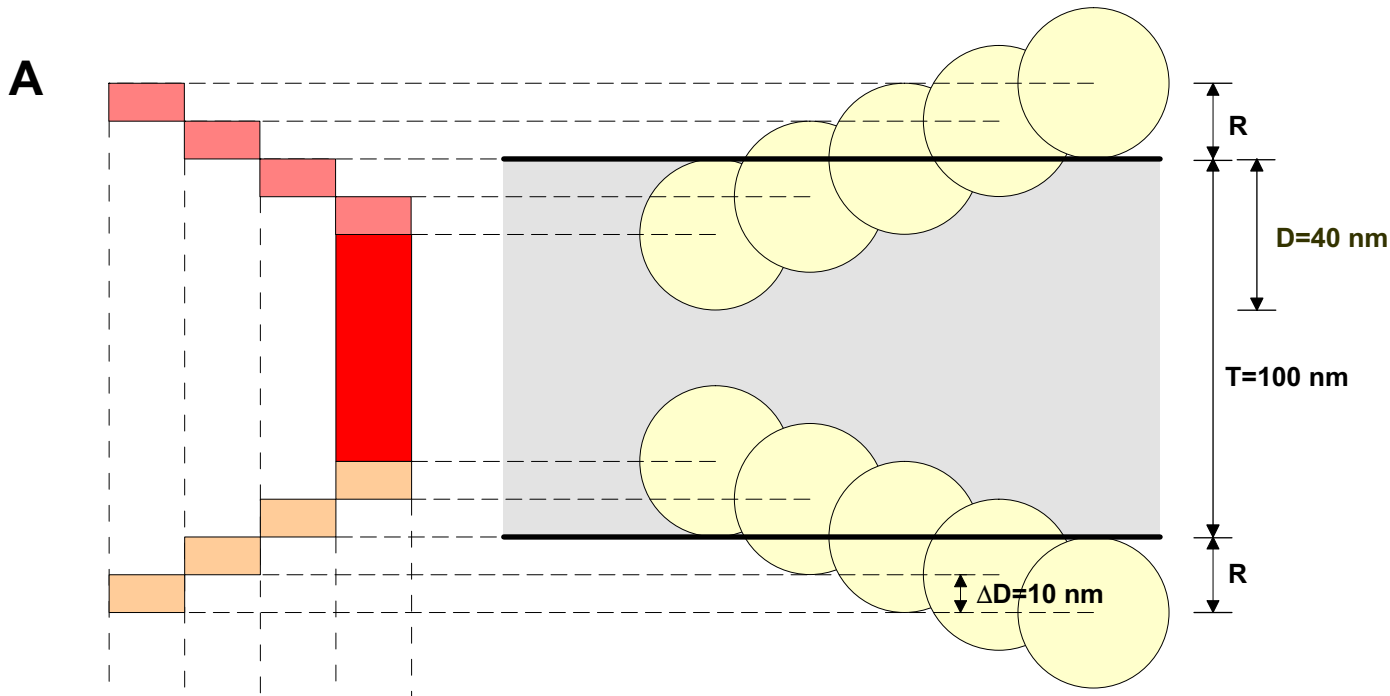

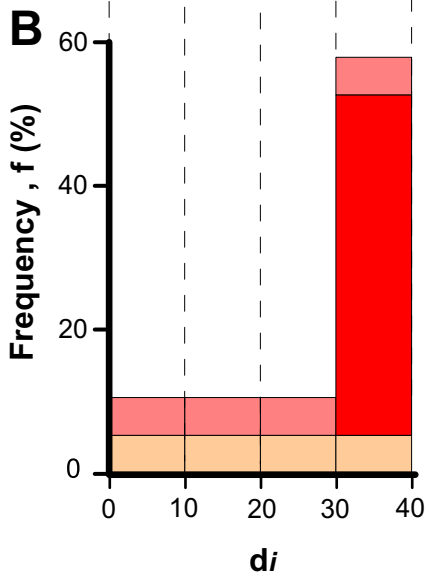

C

f = frequency
D = diameter of object
R = radius of object
T = thickness of section
d*i* = size category

$$d_i = D - i\Delta D \quad \text{where} \left(i = 1 \ldots \frac{D}{\Delta D} \right)$$

for
$D - \Delta D < d_i \leqslant D$

$$f(d_i) = \frac{T - 2R}{T + 2R} + \frac{2\Delta D}{T + 2R} = \frac{T - D + 2\Delta D}{T + D}$$

for
$d_i \leqslant D - \Delta D$

$$f(d_i) = \frac{2\Delta D}{T + 2R} = \frac{2\Delta D}{T + D}$$

Martin S., Figure S7